

Observables and initial conditions for rotating and expanding fireballs with spheroidal symmetryT. Csörgő,^{1,2} M. I. Nagy,³ and I. F. Barna¹¹*MTA Wigner FK, P.O. Box 49, H-1525 Budapest 114, Hungary*²*KRF, Mátrai út 36, H-3200 Gyöngyös, Hungary*³*ELTE, Pázmány Péter Sétány 1/A, H-1118 Budapest XI, Hungary*

(Received 18 November 2015; published 25 February 2016)

Utilizing a recently found class of exact, analytic rotating solutions of nonrelativistic fireball hydrodynamics, we calculate analytically the single-particle spectra, the elliptic flows, and two-particle Bose-Einstein correlation functions for rotating and expanding fireballs with spheroidal symmetry. We demonstrate that rotation generates final state momentum anisotropies even for a spatially symmetric, spherical initial geometry of the fireball. The mass dependence of the effective temperatures as well as the Hanbury Brown–Twiss (HBT) radius parameters and the elliptic flow are shown to be sensitive not only to radial flow effects but also to the magnitude of the initial angular momentum.

DOI: [10.1103/PhysRevC.93.024916](https://doi.org/10.1103/PhysRevC.93.024916)**I. INTRODUCTION**

In noncentral heavy ion collisions, the impact parameter is non-vanishing, and the initial conditions include a nonvanishing but frequently neglected initial angular momentum of the nucleons that participate in the inelastic collisions. This nonzero initial angular momentum of the participant zone is a conserved quantity that survives the initial, nonequilibrium stage of the heavy ion collision, which results in thermalization. The fireballs created in noncentral high energy heavy ion collisions will thus not only expand but rotate as well. The vast majority of numerical and analytic hydrodynamical calculations performed so far completely neglected the effect of the initial angular momentum on the final state observables. The effects of rotation, however, may be rather significant and, rather recently, the imprints of rotation on the observables started to draw significant theoretical attention.

As far as we know, the initial angular momentum of noncentral heavy ion collisions was first taken into account in Ref. [1], where a sign change of the directed flow v_1 was predicted. This was related to an increased importance of the angular momentum driven expansion as compared to the pressure given radial expansion at LHC energies. The rotation effect was also related to a rapidity dependent oscillating pattern of the elliptic flows when these were corrected [1] for the fluctuations of the initial center-of-mass rapidity. These results were highlighted as an important feature of the description of the nearly perfect fluids formed in high energy heavy ion reactions at Relativistic Heavy Ion Collider (RHIC) and Large Hadron Collider (LHC) energies using a numerical hydrodynamical model, that is based on the particle-in-cell method [2]. This hydrodynamical model is a three-dimensional, finite calculation, and it was tested against numerical viscosity and entropy production artifacts [1]. The finiteness of the fireball is an important requirement, when rotation effects are considered, given that models that assume longitudinal boost invariance and flat rapidity dependence have infinite moment of inertia in the beam direction, hence they cannot, by definition, take into account the explosion and simultaneous rotation of the fireball in the impact parameter plane: such a rotation would require a finite moment of inertia.

The differential two-particle Bose-Einstein or Hanbury Brown–Twiss correlation function (DHBHT) was proposed as an effective tool to measure the angular momentum of noncentral heavy ion collisions [3]. The results detailed in Ref. [4] indicated that the DHBHT method can indeed be used to detect the angular momentum and the rotation of the fireball, but the effects of irregular initial shapes, density fluctuations, irregular radial flows require extended analysis to disentangle these effects from one another. The differential correlation function was numerically found to depend on the shape, the temperature, the radial velocity, and the angular velocity as well as on the detector position, as demonstrated in Ref. [5], and the numerical value of the DHBHT correlation function for realistic angular velocities and radial flows was found to be rather small, of the order of 2–3%. Increased initial angular momentum of the rotating and expanding fireball was shown to result in an effective decrease of the observable correlation radii in Ref. [6].

These numerical evaluations of observable signals of a nonvanishing initial angular momentum were partially based on a recently discovered family of exact solutions of rotating and expanding, nonrelativistic fireball hydrodynamics, detailed in Ref. [7]. This solution with nonvanishing initial angular momentum can be considered as the rotating and spheroidally symmetric generalization of the radially expanding, finite, Gaussian exact solution of fireball hydrodynamics found already in 1998 [8]. That solution was shown to be a simultaneous solution of the equations of nonrelativistic fireball hydrodynamics with spheroidal symmetry, and, at the same time, also a solution of the nonrelativistic form of the collisionless Boltzmann equation. The first relativistic solution of fireball hydrodynamics for rotating fluids was found by generalizing this method of Ref. [8] to relativistic kinematics, i.e., looking for those families of solutions of relativistic fireball hydrodynamics that also simultaneously solve the collisionless relativistic Boltzmann equation [9]. It is interesting to note that several families of exact, rotating hydrodynamical solutions were found in this class, for example rotating Hubble flows and rotating but asymptotically non-Hubble flows as well. Hatta, Noronha, and Xie rediscovered these solutions independently and generalized them also for axially symmetric, expanding fireballs with nonvanishing

viscosity [10], carrying out a systematic search using anti-de Sitter conformal field theory (AdS-CFT) correspondence techniques for similar solutions as well [11]. The influence of a nonvanishing initial angular momentum was also investigated in the holographic picture of quark gluon plasma [12], pointing out that the estimates of quark chemical potential can be considerably improved by taking the angular momentum conservation into account. The quickly developing field of exact and analytic solutions of rotating fireball hydrodynamics was briefly reviewed in Ref. [13], which also discussed recent efforts to consistently derive and formulate the theory of viscous relativistic hydrodynamics, and emphasized the conceptual difficulties that relate to the application of the hydrodynamical method to high energy heavy ion collisions, summarizing at the same time the enormous successes of the hydrodynamical models at RHIC and LHC energies.

Due to the conservation of angular momentum, and assuming the validity of certain kind of equipartition theorem, Ref. [14] predicted that the Λ and $\bar{\Lambda}$ baryons emerge from the noncentral heavy ion collisions in a polarized manner. Using numerical hydrodynamical calculations as well as the analytic approach of Ref. [8], the Λ polarization was evaluated by taking into account both the radial expansion and the rotation effect simultaneously [15], and an observable amount of Λ polarization was predicted. In addition, Ref. [16] evaluated the vorticity from the exact rotating solutions and pointed out, together with Ref. [17], the importance of the Kelvin-Helmholtz instability in the initial stages of the fireball evolution. In Ref. [18] the vorticity of the expanding matter was estimated using a transport model simulation.

Despite these theoretical efforts, as far as we know, the ongoing experimental studies have not yet separated the angular momentum effects from radial flow effects on spectra, elliptic flow, and Bose-Einstein correlations, partly because there has been a lack of clear theoretical understanding of how the nonvanishing value of the initial angular momentum influences the final state observables, which are typically measured and interpreted as variables sensitive to radial flows. Elliptic flows are particularly interesting observables that are deeply connected to the fluid nature of the quark matter created in heavy ion collisions. They are frequently interpreted in terms of pressure gradients and radial flows, which convert the initial spatial anisotropy to final state momentum space anisotropy.

In this manuscript, we consider the case of the recently found analytic, exact solutions of nonrelativistic fireball hydrodynamics [7], which describe rotating expansions with spheroidal symmetry. In particular we consider rotating expansions of a spheroid, where the spheroid under investigation is an ellipsoid whose principal axes perpendicular to the angular momentum are equal. Our main goal is to clearly demonstrate the influence of the initial conditions, in particular the nonvanishing value of the initial angular momentum of the fireball, on the final state observables. Utilizing this solution, we derive simple and straightforward analytic formulae that provide a possibility to experimentally test the effects of rotation on fireball hydrodynamics. We also investigate the dependence of the observables on the freeze-out temperature. Although our treatment of the rotation of the expanding fireball in heavy-ion collisions definitely oversimplifies the physical

situation of noncentral heavy ion collisions, to our knowledge this is the first successful attempt to analytically determine the effect of the rotation on the single-particle spectra, elliptic flow, and HBT radii for finite, expanding fireballs.

The structure of this manuscript is as follows. In Sec. II we recapitulate the rotating and expanding solution of fireball hydrodynamics that we use for the evaluation of the observables and present a generalization of its first integrals of motion. In Sec. III we derive the analytic formulae that describe the single-particle spectra, elliptic and higher order flows, as well as the various azimuthally sensitive HBT radii for this family of rotating and expanding exact solutions of fireball hydrodynamics. We illustrate the analytic results also by numerical calculations of an exploding and rotating, initially spherical fireball, and demonstrate how larger and larger initial angular momentum may influence more and more the slope of the single-particle spectra, as well as the particle mass and transverse momentum dependence of the elliptic flow and the azimuthally sensitive HBT radii. Finally, we summarize and conclude.

For the sake of completeness, the manuscript is closed by two Appendices. Appendix A details how we reduce the evaluation of the observables from these rotating solutions of fireball hydrodynamics to integration by quadratures, and gives the conditions of validity for these derivations. To advance the knowledge of possible hydrodynamical solutions that might be useful for future applications in high-energy physics, we close the presentation with a survey of some recent developments in analytic solutions of hydrodynamics in Appendix B.

II. A ROTATING HYDRODYNAMICAL SOLUTION

Following Ref. [7], we outline the hydrodynamical solution valid for rotating expanding spheroids, which allows us to analytically evaluate the observables. The hydrodynamical problem is specified by the continuity, Euler, and energy equations:

$$\partial_t n + \nabla(n\mathbf{v}) = 0, \quad (1)$$

$$\partial_t \mathbf{v} + (\mathbf{v}\nabla)\mathbf{v} = -\nabla p/(m_0 n), \quad (2)$$

$$\partial_t \varepsilon + \nabla(\varepsilon\mathbf{v}) = -p(\nabla\mathbf{v}), \quad (3)$$

where n denotes the particle number density, m_0 is the mass of an individual particle (dominating the equation of state), \mathbf{v} stands for the nonrelativistic (NR) flow velocity field, ε is the NR energy density, and p is the pressure. This set of equations (1)–(3) expresses five equations for six unknowns, and is closed by some equation of state (EoS) that provides a relation among pressure, energy, and number density; this relation can be naturally expressed through their dependences on the temperature T . Just as in Refs. [7,19], we choose a family of generalized equations of state as

$$p = nT, \quad \varepsilon = \kappa(T)nT. \quad (4)$$

This EoS allows us to study the solutions of NR hydrodynamical equations for any temperature-dependent ratio of pressure to energy density, $p/\varepsilon = 1/\kappa(T)$, if the fireball evolution is also characterized by a conserved particle number n . This approximation may be realistic if, in the final stages of the hydrodynamical evolution, the hadrochemical reactions that may change the particle types are closed at temperatures above the

kinetic freeze-out temperature. Such an assumption is favored by data [20,21] and is frequently used in the phenomenology of high energy heavy ion collisions. For a recent overview of the application of the concept of chemical freeze-out at or near to the quark-hadron phase boundary, see, e.g., Ref. [22].

The above EoS is thermodynamically consistent for any function $\kappa(T)$, as was shown in Ref. [19]. The introduction of the function $\kappa(T)$ as above contains several well-known special cases: a nonrelativistic ideal gas has $\kappa(T) = 3/2$, while for a gas of relativistic massless particles one has $\kappa = 3$. Also, one can incorporate a parametrization of the low temperature limit (after the hadrochemical freeze-out) of the lattice QCD equation of state into a suitable $\kappa(T)$ function. One also can model the change of the p/ε ratio at a phase transition from deconfined quark matter to hadronic matter, if one wants to follow the time evolution from very high initial temperatures that corresponds to deconfined quark matter, following the lines of Ref. [7], in which case the conserved charge density has to be replaced by the entropy density σ and the enthalpy density $\varepsilon + p = \mu n + T\sigma$ will be dominated by the second term, $\varepsilon + p \approx T\sigma$. However, the hadronic observables evaluated in the subsequent parts of this manuscript are formed in the final stages of the hydrodynamical evolution, so we assume that the particle identity changing hadrochemical reactions can be neglected close to the kinetic freeze-out temperature, and we proceed with the evaluation of the observables in the approximation $\varepsilon + p \approx m_0 n$. Note also that one usually introduces the speed of sound as $c_s^2 = dp/d\varepsilon = 1/\kappa(T)$. Thus the above EoS allows for any temperature-dependent speed of sound, which can be taken either from measurements or from fundamental calculations. Note also that the dynamics of rotating and expanding fireballs was also considered for even more general equations of state, where only the local conservation of entropy density can be assumed but the chemical potential is vanishing, so the enthalpy density is dominated by the $T\sigma \gg \mu n$ term. This approximation, $\varepsilon + p \approx T\sigma$, is relevant, e.g., in the case of lattice QCD calculations for the equations of state, and the effect on the dynamics of fireball explosiveness has been evaluated and discussed already in Ref. [7]. Here we consider massive particles driving the expansion as we focus on the dynamics around the freeze-out time, which are relevant for the evaluation of the hadronic observables.

From now on, let us consider n , \mathbf{v} , and T as the independent unknown functions, keeping in mind the caveats mentioned above and discussed also in Ref. [7]. The hydrodynamical equations are solved similarly as in the case of a nonrotating, NR ideal gas in Ref. [19], by the following self-similar, ellipsoidally symmetric density profile and the corresponding velocity profile, which describe the dynamics of a rotating and expanding fireball [7]:

$$T(\mathbf{r},t) = T(t), \quad (5)$$

$$n(\mathbf{r},t) = n_0 \frac{V_0}{V} \exp \left\{ -\frac{r_x^2}{2X^2} - \frac{r_y^2}{2Y^2} - \frac{r_z^2}{2Z^2} \right\}, \quad (6)$$

$$\mathbf{v}(\mathbf{r},t) = \left(\frac{\dot{X}}{X} r_x + \omega r_z, \frac{\dot{Y}}{Y} r_y, \frac{\dot{Z}}{Z} r_z - \omega r_x \right). \quad (7)$$

Here $\omega = \omega(t)$ is the (time-dependent) magnitude of the angular velocity, and the scale parameters (the magnitudes of the ellipsoid axes) are denoted by $(X, Y, Z) = (X(t), Y(t), Z(t))$, and the time dependence of the variables is suppressed. In addition, \dot{A} stands for the time derivative of a time-dependent A function: $\dot{A} = \frac{d}{dt} A(t)$ and \ddot{A} stands for the time derivative of \dot{A} . The quantity V is a measure of the volume of the expanding system: $V = (2\pi)^{3/2} XYZ$.¹ The initial values of the temperature and this volume are then denoted by $T_0 = T(t_0)$, $V_0 = V(t_0)$; while the n_0 quantity is a constant, corresponding to the initial value of the density in the center.

Note that, compared to Ref. [7], we changed the labeling of the axes: to correspond to the usual notation in heavy-ion physics, in this paper we take the r_z axis to be parallel with the beam axis, and the event plane (the plane spanned by the impact parameter vector and the beam axis) is assumed to be the (r_x, r_z) plane. The rotation of the expanding fireball is then assumed to be around the r_y axis, because the initial angular momentum points in this direction, while in Ref. [7] the axis of rotation was denoted by r_z .

In Ref. [7] it is shown that the above *Ansatz* for the temperature, velocity, and density fields indeed yields a solution to the hydrodynamical equations if the following conditions are met. It turns out that only ‘‘spheroidally symmetric’’ solutions, i.e., solutions with $X(t) = Z(t) \equiv R(t)$ have been described so far in this way. The time evolution of the radius parameters $X = Z = R$, the vertical scale parameter Y , the temperature T , and the angular velocity ω are governed by the following ordinary differential equations:

$$X = Z \equiv R, \quad (8)$$

$$\dot{X} = \dot{Z} \equiv \dot{R}, \quad (9)$$

$$R\ddot{R} - R^2\omega^2 = \ddot{Y}Y = \frac{T}{m_0}, \quad (10)$$

$$\dot{T} \frac{d}{dT} (T\kappa(T)) = -T \frac{\dot{V}}{V}, \quad (11)$$

$$\omega = \omega_0 \frac{R_0^2}{R^2}. \quad (12)$$

The above formulas generalize the dynamical equations of Ref. [19] for the case of nonvanishing initial angular momentum, characterized here by the initial value of the angular velocity ω_0 , and for spheroidal ($X = Z = R$) expansions. For a vanishing value of the initial angular momentum, $\omega_0 = 0$, the results of Ref. [19] are reproduced on the level of the dynamical equations that characterize the expansion of the scale parameters (X, Y, Z) , except the tilt angle, which was introduced in Ref. [19] to characterize phenomenologically, with a time-independent constant angle, the effect of the rotation of the principal axis of the expanding ellipsoid in the impact parameter plane with respect to the direction of the beam. In Ref. [19] it was argued that, due to the expanding

¹We have included in the definition of the volume a constant of integration $(2\pi)^{3/2}$, so that the total number of particles N is given by the volume integral of the density n , which yields $N = n_0 V_0$ as a constant of the motion.

nature of the fireball, the moment of inertia increases for late stages of the expansion, so the angular velocity slows down due to the conservation of angular momentum. Hence, in the final stages of the expansion, approximately, a constant value of the tilt angle can be used to evaluate the observables.

By now, we are able to solve the dynamical equations that describe the rotation of the fireball in the impact parameter plane, and so the tilt angle $\vartheta = \vartheta(t)$ and the angular velocity $\omega = \dot{\vartheta}$ in this article are both time-dependent functions, which can be evaluated for the expanding and rotating ellipsoid by integrating the time-dependent angular velocity as follows:

$$\vartheta = \vartheta_0 + \int_{t_0}^t dt' \omega(t'). \quad (13)$$

Following Ref. [19], the temperature equation (11) can also be integrated as

$$\frac{V_0}{V} = \exp[\kappa(T) - \kappa(T_0)] \exp \int_{T_0}^T \frac{dT'}{T'} \kappa(T'), \quad (14)$$

and in the case of temperature-independent κ , i.e., $\kappa(T) = \kappa = \text{const}$, this relation can be expressed in the simple and instructive way as

$$T = T_0 \left(\frac{V_0}{V} \right)^{1/\kappa}. \quad (15)$$

This equation is formally the same as the temperature law for adiabatic expansions of homogeneous gases of volume V , where $TV^{\gamma-1} = \text{const}$, and the adiabatic index is introduced as $\gamma = (f+2)/f$, where f stands for the elementary degrees of freedom. Identifying the adiabatic index γ with $1 + 1/\kappa$, one obtains the relation $f = 2\kappa$, so one can relate the coefficient between the energy density and the pressure to the number of degrees of freedom in the manner usual in thermodynamics of ideal gases. In our particular case, $\kappa \equiv \kappa(T)$ is a temperature-dependent function, and so is the effective number of degrees of freedom, $f \equiv 2\kappa(T)$. Let us also emphasize that we discuss an exact solution of a rotating and expanding hydrodynamical system, where the density, the velocity, and the pressure fields are all functions of space and time, so the emergence of the law of adiabatic expansions of thermodynamics is a beautiful byproduct of the fact that we were able to reduce the complicated system of partial differential equations of hydrodynamics to a system of coupled, nonlinear but ordinary differential equations. In this particular case, the occurrence of the law of adiabatic expansions of thermodynamics corresponds precisely to the adiabatic or perfect fluid nature of the exploding and rotating Gaussian fireball under investigation.

The time evolution of the principal axes R and Y is given by Eq. (10), which can be understood as a classical motion of a point particle with mass m in a noncentral potential. The corresponding Hamiltonian $H(P_R, P_Y, R, Y)$ takes a simple form in the $\kappa = \text{const}$ case:²

$$H = \frac{P_R^2 + 2P_Y^2}{4m_0} + \frac{m_0\omega_0^2 R_0^4}{R^2} + T_0\kappa \left(\frac{R_0^2 Y_0}{R^2 Y} \right)^{1/\kappa}, \quad (16)$$

²Reference [7] details the Hamiltonians for other choices of the $\kappa(T)$ function, or for the case when there is no conserved charge n .

from which $P_R = 2m_0\dot{R}$, $P_Y = m_0\dot{Y}$ follows. One can verify that the Hamiltonian equations of motion are indeed the ones in Eq. (10). A first integral of the motion is simply the conservation of the energy E :

$$\frac{E}{m_0} = \dot{R}^2 + \frac{\dot{Y}^2}{2} + \frac{\omega_0^2 R_0^4}{R^2} + \frac{T_0\kappa}{m} \left(\frac{R_0^2 Y_0}{R^2 Y} \right)^{1/\kappa} = \text{const.}$$

This equation, with the help of the form of the solutions for the temperature T and the angular momentum ω , can also be rewritten in the following, rather intuitive form:

$$E = m_0 \left(\dot{R}^2 + \frac{\dot{Y}^2}{2} + \omega^2 R^2 \right) + \kappa T, \quad (17)$$

which indicates that the dependence of the temperature on the volume $V = (2\pi)^{3/2} R^2 Z$ plays the role of an effective, noncentral potential in the corresponding Hamiltonian problem. If the special case $\kappa = 3/2$ is considered (this is the case of a classical ideal gas), the Hamiltonian problem can be solved using quadratures; see Appendix A for the details. An interesting result is that in this case the time dependence of the $2R^2 + Y^2$ quantity can be expressed explicitly for arbitrary initial conditions:

$$2R^2 + Y^2 = 2(\dot{R}_0 t + R_0)^2 + (\dot{Y}_0 t + Y_0)^2 + \left(\frac{3T_0}{m_0} + 2\omega_0^2 R_0^2 \right) t^2. \quad (18)$$

This formula generalizes the earlier results of Refs. [19,24,30] for the case of nonvanishing initial angular momentum, characterized here by the initial value of the angular velocity ω_0 . For a vanishing value of ω_0 , and for the spheroidal expansions of $X = Z = R$, the earlier results of Refs. [19,24,30] are reproduced.

For other choices of κ , one has to resort to numerical solutions of Eq. (10), the equation of motion. Such solutions can be easily found numerically for any initial conditions R_0 , Y_0 , \dot{R}_0 , \dot{Y}_0 , T_0 , and ω_0 with the presently available tools of desktop mathematics (e.g., MAPLE, MATLAB, or MATHEMATICA).

III. OBSERVABLES FROM THE NEW SOLUTION

In the previous section we have seen how the hydrodynamical equations of a rotating and spheroidally symmetric, expanding fireball can be reduced to an easily solvable system of ordinary differential equations, and we have also derived some new first integrals of the motion. To obtain some physically interesting particular solutions, one needs to specify the equations of state, the initial conditions, and the freeze-out conditions. In this manner, one can easily investigate the effect of rotation on the time evolution of the system. In this section we illustrate this dynamics with some examples and proceed with the analytic evaluation of the observables from the dynamical solutions; then we illustrate these analytic results with some numerical examples.

For the sake of illustration, we take the initial conditions to be that of a sphere, with $X_0 = Z_0 \equiv R_0 = 5$ fm, $Y_0 = 5$ fm, and $T_0 = 350$ MeV. For the sake of simplicity, we switch off the effects of initial radial flows, $\dot{X}_0 = \dot{Z}_0 = \dot{R}_0 = 0$, because in these numerical examples we focus on the effects of initial

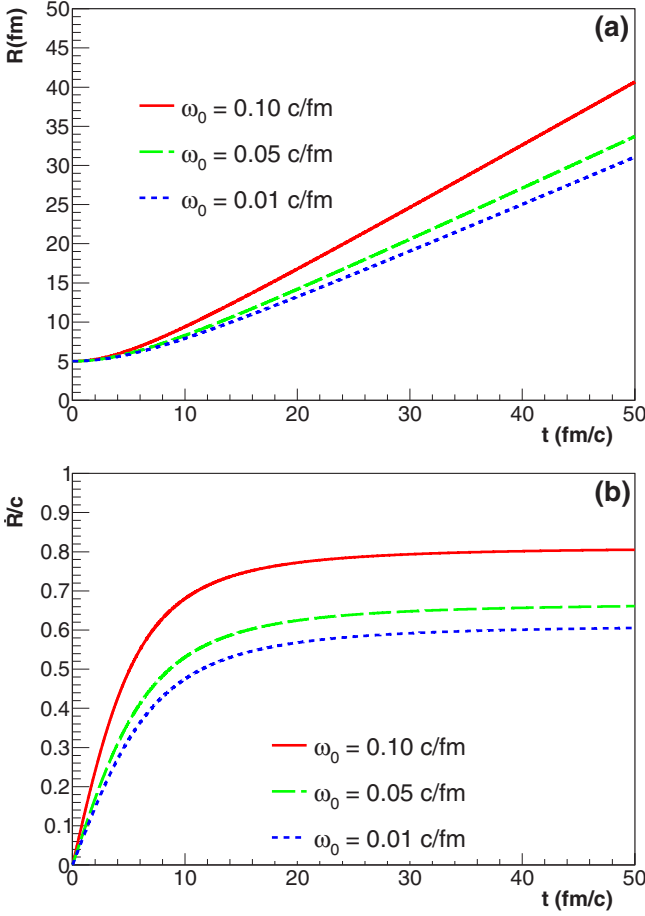


FIG. 1. Time evolution of the axes $X(t) = Z(t) \equiv R(t)$ (a) and the corresponding velocity $\dot{R}(t)$ (b) for our hydrodynamical model in three cases of ω_0 . Initial conditions are $R_0 = 5$ fm, $Y_0 = 5$ fm, $\dot{R} = \dot{Y} = 0$, $T_0 = 350$ MeV. One sees that increased initial angular momentum leads to increased, more violent explosion in the radial direction.

angular momentum, which can be demonstrated more clearly if the interference with radial flow effects (inherent in the formulas) is switched off for the purpose of these numerical examples. We compare three cases, each of different initial angular momentum, corresponding to ω_0 values increasing gradually from nearly zero to a more realistic value of 0.1 c/fm. For the sake of these illustrations, we take the simple $\kappa = 3/2$ value for the EoS and expect qualitatively similar results for other choices of the $\kappa(T)$ function, and we set the m_0 parameter of the dynamical equations of motion to be the proton mass, $m_0 = 938$ MeV. As it was shown in Ref. [17], the dynamics of the numerical solution of a (1+3)-dimensional fireball hydrodynamical problem with lattice QCD equation of state is well approximated with our simple analytic fireball hydrodynamic solution from [7], used to model the dynamics also in our present article.

Figures 1, 2, and 3 show the time evolution of the $X(t) = Z(t) \equiv R(t)$ and the $Y(t)$ axes, the temperature, and the angular velocity, respectively. One indeed sees what one expects, based on the analytic structure of the dynamical equations of Eqs. (8)–(12), namely that increased initial angular momentum

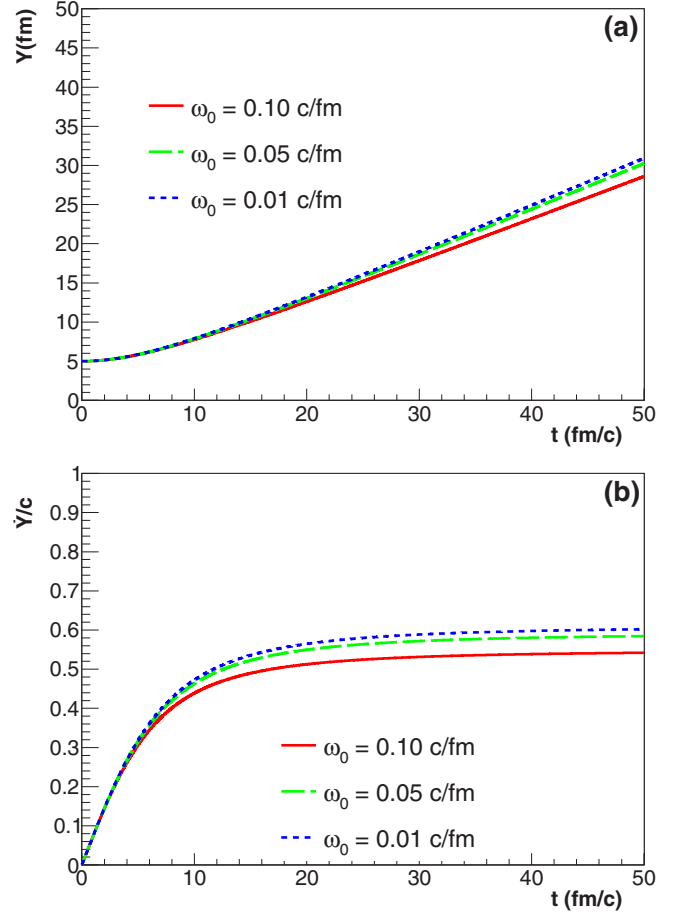


FIG. 2. Time evolution of the $Y(t)$ axis (a) and $\dot{Y}(t)$ (b) for our hydrodynamical model in three cases of ω_0 . Initial conditions are the same as in Fig. 1. The more violent radial expansion related to increased values of initial angular momentum results in decreased expansion in the Y direction, due to the faster cooling and the correspondingly faster decrease of the pressure of the fireball.

leads to an accelerated expansion in the R direction, and faster cooling, and this leads to a slightly decreased expansion in the Y direction. However, it is also evident in these plots that the nonrelativistic approximation is not too realistic for our initial conditions: the velocity of the principal axes reaches the order of magnitude where a relativistic treatment would be needed.

In order to evaluate the measurable quantities from the hydrodynamical solution, a further specification needs to be made: namely, the condition of the freeze-out (that sets the end of the hydrodynamical evolution) has to be stated. Let us introduce the f subscript to indicate that the quantity is to be taken at the freeze-out time, t_f . Here we assume that, when the temperature reaches a given T_f value, a sudden freeze-out happens, and identical particles with mass m are produced. We evaluate some of the observables for pions, kaons, and protons or antiprotons, where for the observed particles we use $m = 140, 494,$ and 938 MeV, respectively.

The $T_f \equiv T(t_f)$ temperature is reached everywhere at the same time t_f in the considered class of solutions, as seen from

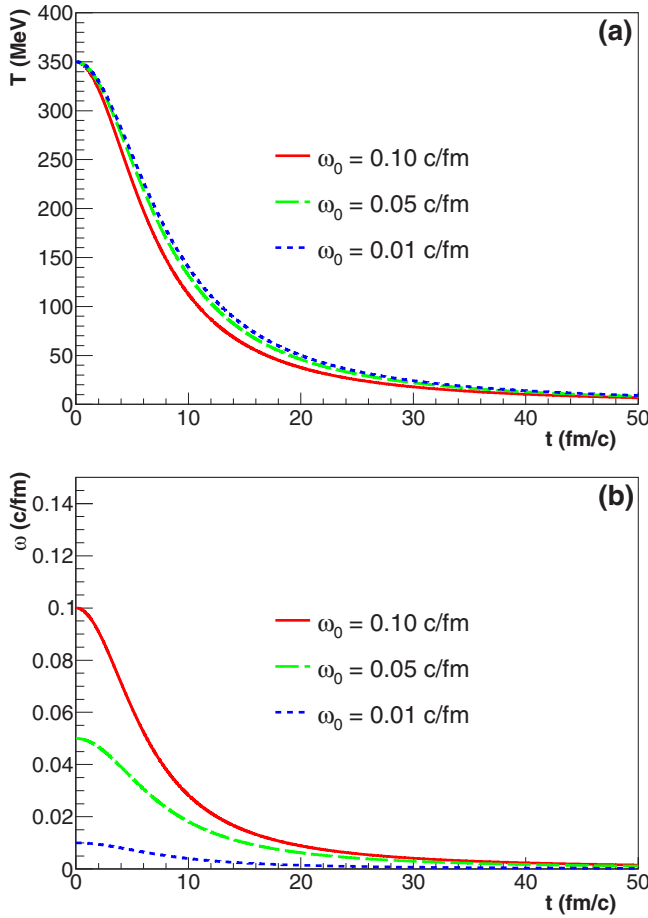


FIG. 3. Time evolution of the temperature (a) and the angular velocity (b) for our hydrodynamical model in three cases of ω_0 . In this demonstrational case, $\kappa = 3/2$, so the temperature is directly related to the geometrical size of the fireball through Eq. (15). Initial conditions are the same as in Fig. 1. Larger initial angular momentum leads to faster radial expansion, which causes faster cooling. In this class of rotating and expanding, spheroidal fireball solutions, the time evolution of the r_y component of the vorticity vector, $\omega_y(t)$, equals twice the angular velocity $\omega(t)$, indicated in the lower panel, due to Eq. (23).

Eq. (5). The emission function can be written as

$$S(t, \mathbf{r}, \mathbf{p}) = \frac{n}{(2\pi mT)^{3/2}} \exp\left\{-\frac{(\mathbf{p} - m\mathbf{v})^2}{2mT}\right\} \delta(t - t_f), \quad (19)$$

where the space and time dependence of the \mathbf{v}, T, n fields was suppressed in the notation. This emission function is normalized so that its integral over \mathbf{p} at a given point \mathbf{r} indeed yields the number density n at that point. We also assume that at freeze-out the equation of state tends to that of an ideal gas: $\lim_{T \rightarrow T_f} \kappa(T) = 3/2$. Using our forms for the \mathbf{v}, T, n fields specified above in Eqs. (7), (6), and (5), one finds that the emission function has a multivariate Gaussian form, and the integrals can be performed analytically.

The effect of the rotation on the expansion dynamics is illustrated on Figs. 1, 2, and 3, which indicate the time evolution of an initially spherical, rotating volume with the same initial geometry $X_0 = Y_0 = Z_0$, without initial radial

flows, $\dot{X}_0 = \dot{Y}_0 = \dot{Z}_0 = 0$, and the same initial temperature T_0 but with various initial angular momenta ω_0 increasing from 0 to 0.1 c/fm. In Fig. 1 one sees that the fluid gains more radial flow with increasing initial angular momentum. The nonrelativistic nature of the solution utilized in this manuscript clearly has its limitations, since we also see in Fig. 1 that the expansion velocity of the two equal principal axes $X = Z \equiv R$ approaches quickly a considerable fraction of the speed of light for the chosen (in some sense realistic) initial conditions.

Figure 2 indicates that the more violent radial expansion in the cases with bigger angular momentum causes slower expansion in the Y direction. Just as for the R direction, we see also here that the example is not realistic in the sense that it cannot be applied to data analysis: the expansion velocities in the out-of-reaction plain direction also quickly reach the relativistic domain when the nonrelativistic approximation breaks down for realistically high initial temperatures and initial angular velocities.

Figure 3 indicates that the temperature of the fireball cools faster with more rotation, which is a direct consequence of the faster increase of the volume of the fireball with increasing initial angular momentum. In our calculations of the observables, we took $T_f = 140$ MeV freeze-out temperature (see Sec. III), which is reached after approximately 8–10 fm/c time, depending weakly on the initial angular momentum, as illustrated in Fig. 3.

Let us introduce the following notation:

$$\begin{aligned} T_x &= T_f + m(\dot{X}_f^2 + \omega_f^2 Z_f^2) \\ &= T_f + m(\dot{R}_f^2 + \omega_f^2 R_f^2), \end{aligned} \quad (20)$$

$$T_y = T_f + m\dot{Y}_f^2, \quad (21)$$

$$\begin{aligned} T_z &= T_f + m(\dot{Z}_f^2 + \omega_f^2 X_f^2) \\ &= T_f + m(\dot{R}_f^2 + \omega_f^2 R_f^2). \end{aligned} \quad (22)$$

We chose the x, y, z subscripts to denote the principal directions and also the X, Y, Z notation to denote the size of the axis of the expanding spheroid in the corresponding principal directions for the sake of clarity and consistency with earlier results, but remember that in the present solution $X = Z$, so $\dot{X} = \dot{Z}$, and $T_x = T_z$. Based on the effect of the rotation on the expansion dynamics as illustrated in Figs. 1, 2, and 3, it is plausible to assume that the initial conditions imply $T_x = T_z > T_y$ in practical cases, when the initial radial flows are expected to be small, $\dot{X} \approx \dot{Z} \approx 0$.

Rotational fluids are frequently characterized in terms of their vorticity vector, defined as $\omega(\mathbf{r}, t) = \nabla \times \mathbf{v}(\mathbf{r}, t)$. For this class of rotating and expanding, spheroidal fireball solutions, the vorticity vector has been found [7] to be spatially homogeneous, pointing to the axis of rotation, and directly proportional to the value of the angular velocity of the fluid, the scalar function $\omega(t)$, that we recapitulate here for the sake of completeness. In the present article the principal axis of the rotation corresponds to the r_y direction, while in Ref. [7] the axis of rotation was pointing to the r_z direction. Hence, in the notation of the current article, the vorticity for this family of rotating and expanding exact solutions of fireball

hydrodynamics is

$$\boldsymbol{\omega}(\mathbf{r}, t) = \nabla \times \mathbf{v}(\mathbf{r}, t) = (0, 2\omega(t), 0). \quad (23)$$

Therefore, the time evolution of the angular velocity $\boldsymbol{\omega} \equiv \omega(t)$, indicated in Fig. 3, equals the time evolution of half of the r_y component of the spatially homogeneous vorticity vector, $\omega_y \equiv \omega_y(t)$:

$$\omega = \frac{1}{2}\omega_y. \quad (24)$$

In what follows, we demonstrate that the parameters T_x and T_y introduced in Eqs. (20)–(22) in this article play a very similar role to that of the analogous variables introduced in Ref. [19]. There, the dynamics of the rotation was not taken into account, consequently the expressions of T_x and T_y lacked the term corresponding to the rotational energy, $R^2\omega^2$ (with $X = Z = R$), but these terms are clearly identified in the present article. This way we prove that in this class of rotating solutions of fireball hydrodynamics the effect of rotation enters the final state in a rather straightforward way: the effects that were usually associated with that of radial flows need to be reconsidered to take the rotation effects also into account.

The presence of rotation changes the time evolution of the system and thus, for a given initial condition, it influences the final state in an involved way. It is thus rather reassuring to find the simple forms of the rotational terms in the expression of the effective temperatures $T_x = T_z$ and T_y , as a manifestation of rotation.

A. Single-particle spectrum

The single-particle spectrum is basically the integral of $S(\mathbf{r}, \mathbf{p})$ over the spatial coordinates. The result is

$$E \frac{dn}{d^3\mathbf{p}} \propto E \exp \left\{ -\frac{p_x^2}{2mT_x} - \frac{p_y^2}{2mT_y} - \frac{p_z^2}{2mT_z} \right\}. \quad (25)$$

Here E is the energy of the particle. In our case, $T_x = T_z$, since $X_f = Z_f$ and $\dot{X}_f = \dot{Z}_f$. In this case the spectrum is rotationally invariant in the x - z plane, so the observables calculated in this way are automatically valid in the laboratory frame as well as the rotated frame of the fluid. However, in the more general, yet to be explored case of a rotating and expanding ellipsoid with three different axes, this statement is generally not true: in that case, the observables calculated in the rest frame of the collision will differ from those measured in the proper frame of the ellipsoid at freeze-out.

The spectrum seen in Eq. (25) generates the following azimuthally averaged single-particle spectrum (p_t stands for transverse momentum):

$$\frac{dn}{2\pi p_t dp_t dp_z} \propto \exp \left(-\frac{p_t^2}{2mT_{\text{eff}}} - \frac{p_z^2}{2mT_z} \right) I_0(w), \quad (26)$$

$$\frac{1}{T_{\text{eff}}} = \frac{1}{2} \left(\frac{1}{T_x} + \frac{1}{T_y} \right), \quad (27)$$

$$w = \frac{p_t^2}{4m} \left(\frac{1}{T_y} - \frac{1}{T_x} \right). \quad (28)$$

Here and in what follows, the modified Bessel function of order n is denoted by $I_n(w)$, which is defined as $I_n(w) = \frac{1}{\pi} \int_0^\pi dz \cos(nz) \exp[w \cos(z)]$.

Just as we did for the time evolution of the system itself (see Figs. 1–3), we demonstrate the observables in the illustrative $X_0 = Y_0 = Z_0 = 5$ fm, $\dot{X}_0 = \dot{Y}_0 = \dot{Z}_0 = 0$, and $T_0 = 350$ MeV case, taken with three different values of initial angular velocity ω_0 , to display the effect of rotation on them.

Figure 4 shows the slope parameters of the single-particle spectrum taken at freeze-out as a function of the particle mass m . This figure indicates that larger initial angular momentum creates angular velocities that add to the radial flow, thus larger initial angular momentum leads to higher slope parameters or effective temperatures in the single-particle spectrum.

In a relativistic generalization or extension, the mass dependence of the slope parameters transforms into the m_T (transverse mass) dependence; see, e.g., Refs. [23–25], so our result on the m dependence can be taken as a preliminary suggestion on the m_T dependence what one might get in a more realistic relativistic approach. In our calculations, from now on we take the freeze-out temperature T_f to be the pion mass, 140 MeV.

The azimuthal dependence of the single-particle spectrum can be encoded in the Fourier components of it; these are called the flow coefficients, and denoted by v_n . They are defined as

$$\frac{dn}{dp_z p_t dp_t d\phi} = \frac{dn}{2\pi dp_z p_t dp_t} \left[1 + 2 \sum_{n=1}^{\infty} v_n \cos(n\phi) \right]. \quad (29)$$

Here v_1 is called the directed flow, v_2 the elliptic flow, and v_3 the third flow. It is important to note that in our simple model all the event planes coincide, and that is where we set the zero of the azimuthal angle; that is why the sinusoidal terms do not appear in Eq. (29).

It turns out that in our model the transverse- and longitudinal momentum dependence of the v_n flow components can be written in terms of the w scaling variable introduced earlier in Eq. (27). Simple calculation leads now to

$$v_{2n+1} = 0, \quad v_{2n} = \frac{I_n(w)}{I_0(w)}. \quad (30)$$

The odd components of the Fourier decomposition vanish. This is an artifact of the spheroidal symmetry of the flow profile—i.e., the X and Z principal axes coincide—and also a practical consequence of the fact that experimentally it is not possible to tag the forward or backward spatial hemisphere: Although the odd v_n -s may be nonvanishing when the spatial integration is limited to certain parts of the source, the experimental situation corresponds to integration over all parts of the source, and due to this reason the odd v_n -s vanish for spheroidally symmetric sources. So the model presented here is not appropriate to describe the nonzero values of the odd momenta of the azimuthal distribution. In the more general case of a triaxial, rotating ellipsoidal expansion (i.e., where $X \neq Z \neq Y$), also discussed after Eq. (25), but not detailed in this article, an angular tilt of the triaxially expanding fireball would imply nonvanishing odd azimuthal moments, with a characteristic

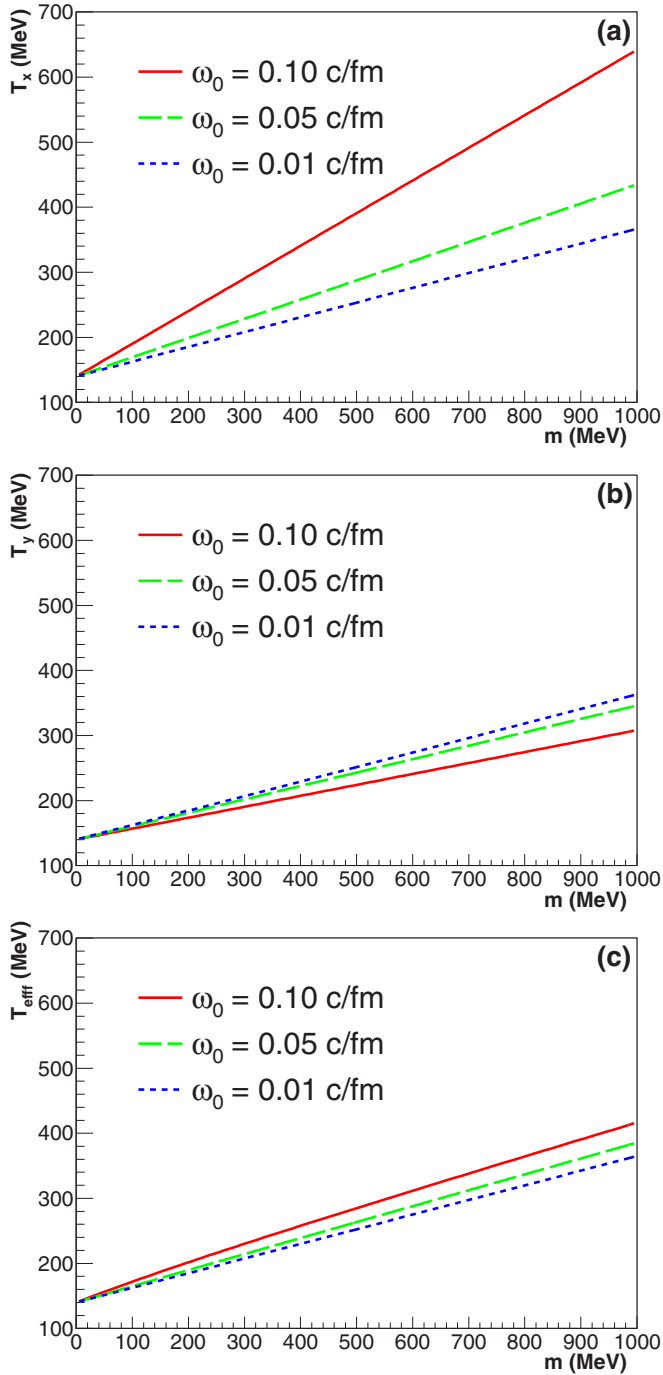


FIG. 4. The slope parameters [$T_x = T_z$ (a), T_y (b)], and the effective temperature introduced in Eq. (27), T_{eff} (c), taken at freeze-out (when T reaches $T_f = 140$ MeV), as a function of particle mass m . As before, three cases of ω_0 are selected for the purpose of demonstration of the analytically obtained formulas. Initial conditions are the same as in Fig. 1.

rapidity dependence, indeed observed in experiment, as this property was seen already for a finite, time-independently tilted, triaxial ellipsoidal expansion in Ref. [19].

However, even in the spheroidal case discussed in this article, the even components mirror the effect of rotation as well: the w variable, which governs the dependence of the

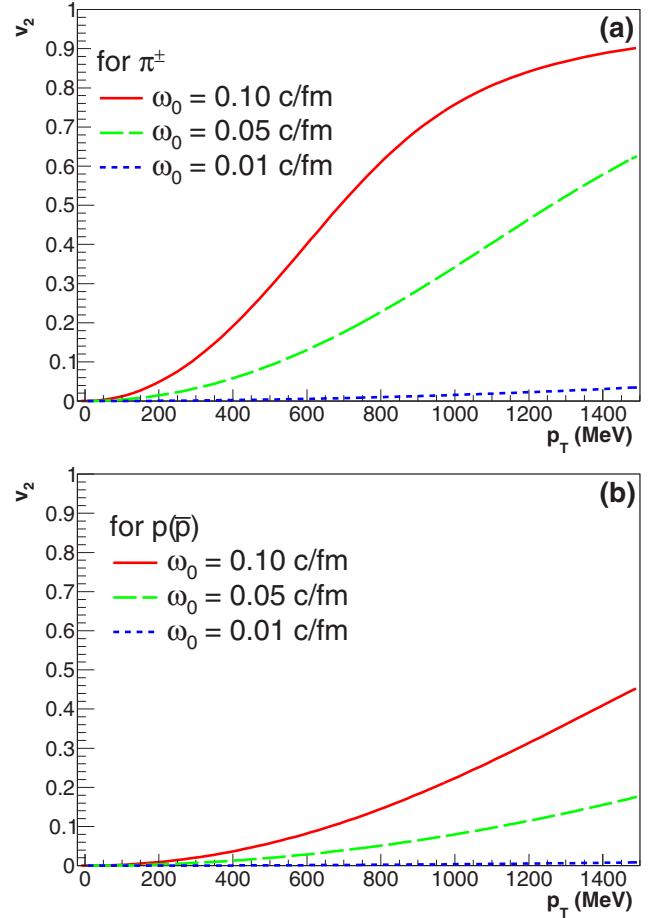


FIG. 5. v_2 for pions (a) and protons (b) as a function of p_T taken at the freeze-out time (when T reaches $T_f = 140$ MeV), for three different ω_0 values. Initial conditions are the same as in Fig. 1. The effect of rotation is clearly the increase of the elliptic flow.

flow components on the kinematic variables,³ and it increases compared to the nonrotating case of Ref. [19], corresponding to the increase of the elliptic flow due to the effect of rotation.

Figures 5 and 6 illustrate again the case of the $X_0 = Y_0 = Z_0 = 5$ fm, $\dot{X}_0 = \dot{Y}_0 = \dot{Z}_0 = 0$, $T_0 = 350$ MeV initial conditions, with three different values of initial angular velocity ω_0 , to see how rotation influences the evolution of the elliptic flow. In this particular case, we emphasize that the initial geometry is spherical, so elliptic flow develops as a dynamical effect entirely due to the angular momentum of an initially spherical volume. In a more realistic situation, where also initial geometrical asymmetries may be present, one thus expects that the elliptic flow also will be quite significantly influenced by the initial angular momentum of the participant zone.

³One should clearly distinguish the angular velocity of the rotating fluid $\omega = \omega(t)$ not only from the vorticity vector, $\omega(\mathbf{r}, t) = \nabla \times \mathbf{v}(\mathbf{r}, t)$, but also from the scaling variable of the elliptic flow, denoted here by w following the notation introduced already in Ref. [19]. The latter scaling w variable enters in this manuscript as the argument of $I_n(w)$.

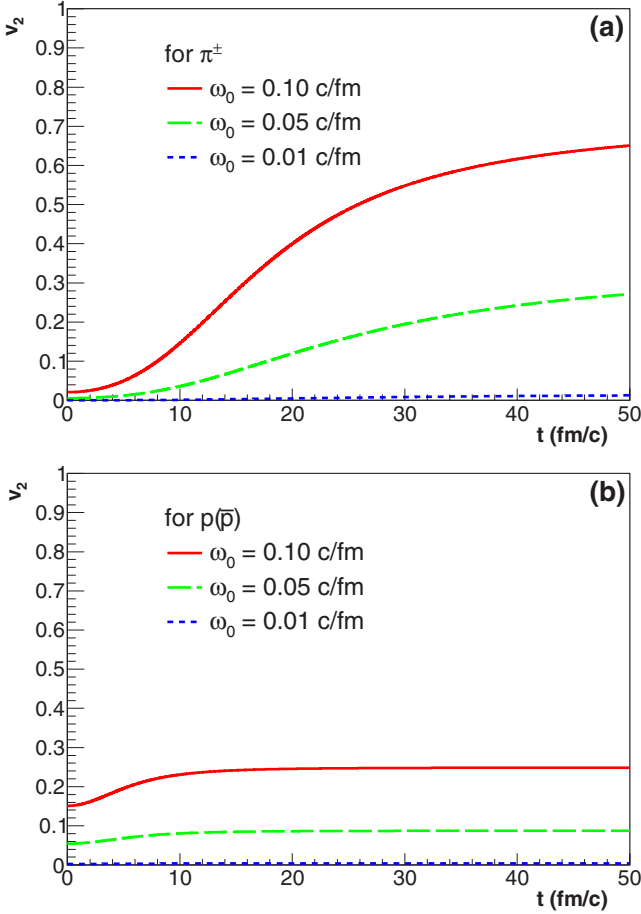


FIG. 6. Freeze-out time dependence of v_2 for pions (a) and protons (b), at a fixed p_T (300 MeV/c for pions and 1000 MeV/c for protons), for three different ω_0 values. Initial conditions are the same as in Fig. 1. The effect of rotation is again seen to increase the elliptic flow.

Figure 5 shows the values of v_2 for pions and protons (to display the effect of particle mass) taken at the freeze-out time, as a function of p_T , while Fig. 6 shows the v_2 of pions and protons for a representative p_T value (300 MeV/c for pions, 1000 MeV/c for protons), as a function of freeze-out time. It is clear that, in this demonstration case of spherically symmetric initial conditions, rotation is what gives v_2 its magnitude. It is also straightforward then to conclude that the nonvanishing initial angular momentum of the participant zone may be an important contributor to the experimentally found and rather significant elliptic flow v_2 of observed particles.

B. Two-particle correlations

The two-particle Bose-Einstein correlation function (BECF) can be calculated from the Fourier transform of the source function $S(t, \mathbf{r}, \mathbf{p})$ of Eq. (19). For an introduction and review on this topic and the evaluation of Bose-Einstein correlation functions from analytic and realistic hydrodynamical models, we recommend [26]. The simplest (spherically symmetric, nonrelativistic, nonrotational) examples for this kind of calculations are given in Refs. [8,27], which we

reproduce here in the special limit of zero initial angular momentum and spherical symmetry. Furthermore, utilizing the core-halo picture [28] one introduces the λ parameter, the effective intercept of the correlation function: $\lambda \equiv \lambda(\mathbf{p}) = [N_c(\mathbf{p})/N(\mathbf{p})]^2$. The λ parameter measures the fraction of particles originating directly from the core, in contrast to those stemming from decay of long-lived resonances. The two-particle correlation function turns out to take the form

$$C(\mathbf{K}, \mathbf{q}) = 1 + \lambda \exp \left\{ -q_x^2 R_x^2 - q_y^2 R_y^2 - q_z^2 R_z^2 \right\}, \quad (31)$$

$$\mathbf{K} = \mathbf{K}_{12} = \frac{1}{2}(\mathbf{p}_1 + \mathbf{p}_2), \quad (32)$$

$$\mathbf{q} = \mathbf{q}_{12} = (\mathbf{p}_1 - \mathbf{p}_2), \quad (33)$$

$$\begin{aligned} R_x^2 &= X_f^2 \left(1 + \frac{m}{T_f} (\dot{X}_f^2 + Z_f^2 \omega_f^2) \right)^{-1} \\ &= R_f^2 \left(1 + \frac{m}{T_f} (\dot{R}_f^2 + R_f^2 \omega_f^2) \right)^{-1}, \end{aligned} \quad (34)$$

$$R_y^2 = Y_f^2 \left(1 + \frac{m}{T_f} \dot{Y}_f^2 \right)^{-1}, \quad (35)$$

$$\begin{aligned} R_z^2 &= Z_f^2 \left(1 + \frac{m}{T_f} (\dot{Z}_f^2 + X_f^2 \omega_f^2) \right)^{-1} \\ &= R_f^2 \left(1 + \frac{m}{T_f} (\dot{R}_f^2 + R_f^2 \omega_f^2) \right)^{-1}. \end{aligned} \quad (36)$$

Remember again that, although we have written these radius parameters in a symmetric way, the spheroidal symmetry of the applied solution, $X = Z$, $\dot{X} = \dot{Z}$, actually implies $R_x = R_z$. These radius parameters can also be called the lengths of homogeneity [29]. Again, note the very simple occurrence of rotational terms in the expression of the radius parameters, just as it was for the slope parameters $T_x = T_z$ and T_y in Eqs. (20) and (22). These terms imply that increased initial angular momentum leads to an enhanced mass dependence and a decrease in the HBT radius parameters. This analytic result yields a deep insight into the earlier, numerically obtained indication that an increased rotation leads to a decreased HBT radius parameter [6].

Up to now we have dealt only with the case when the particle emission happens instantaneously [the delta function in Eq. (19) assures this]. For Bose-Einstein correlations, it is instructive to see what happens when the freeze-out has a small but finite duration time. Let this duration be denoted by Δt . We evaluate the correlation functions by setting the time dependence of the source function equal to $(2\pi \Delta t^2)^{-1/2} \exp[-(t - t_f)^2/2\Delta t^2]$, instead of $\delta(t - t_f)$. Performing the calculation again, one arrives at the conclusion that all the previous radius components, including the cross-terms, are supplemented with an additional term $\delta R_{ij}^2 = \beta_i \beta_j \Delta t^2$, where $\boldsymbol{\beta} = (\mathbf{p}_1 + \mathbf{p}_2)/(E_1 + E_2)$ is the velocity of the pair.

We write the Bose-Einstein correlation functions in a more usual parametrization, the so-called side-out-longitudinal or Bertsch-Pratt (BP) parametrization. In this parametrization, the longitudinal direction $r_{\text{long}} \equiv r_1$ coincides with the beam direction, the “out” direction $r_{\text{out}} \equiv r_o$ is parallel to the mean transverse momentum of the pair in the longitudinal center

of mass system of the pair (LCMS), where $\mathbf{p}_{1z} + \mathbf{p}_{2z} = 0$, and the side direction $r_{\text{side}} = r_s$ is orthogonal to both of these. The mean velocity of the particle pair can be written in the Bertsch-Pratt system as $\boldsymbol{\beta} = (\beta_o, 0, \beta_l)$, where $\beta_o = \beta_r$. We denote by ϕ the angle of the event plane and the mean transverse momentum of the measured pair. Performing the coordinate transformation we obtain the following result:

$$C_2(\mathbf{K}, \mathbf{q}) = 1 + \lambda \exp \left(- \sum_{i,j=s,o,l} q_i q_j R_{ij}^2 \right), \quad (37)$$

$$R_s^2 = R_y^2 \cos^2 \phi + R_x^2 \sin^2 \phi, \quad (38)$$

$$R_o^2 = R_x^2 \cos^2 \phi + R_y^2 \sin^2 \phi + \beta_l^2 \Delta t^2, \quad (39)$$

$$R_l^2 = R_x^2 + \beta_l^2 \Delta t^2, \quad (40)$$

$$R_{ol}^2 = \beta_r \beta_l \Delta t^2, \quad (41)$$

$$R_{os}^2 = (R_x^2 - R_y^2) \cos \phi \sin \phi, \quad (42)$$

$$R_{sl}^2 = 0. \quad (43)$$

These results are simple and straightforward generalizations of the spheroidally symmetric special case of Ref. [19]. As a function of ϕ , many of these radius parameters oscillate. Again, it is important to emphasize that the fact that, e.g., $R_{sl} = 0$, and that $R_{ol} = 0$ for $\Delta t = 0$ is not some general result, but rather an artifact of our considered class of spheroidal solutions where $X = Z$. In a more general case of $X \neq Z$, these cross-terms would appear (as seen, e.g., from the results for a nonrotational but tilted ellipsoid in Ref. [19].) The effect of rotation, however, enters in a very simple way: it results in the decrease of the radius parameters compared to the nonrotating case, as follows analytically from Eqs. (34)–(36) that are related the observable HBT radii through Eqs. (38)–(43). Note, that in the LCMS the mean longitudinal velocity of the pair, $\beta_l = 0$, hence R_l in Eq. (40) will have a vanishing contribution from the duration of the particle emission, and the out-long cross-term of Eq. (41) will also vanish in the LCMS.

It is necessary to note that, in the nonrelativistic model investigated in this work, we see that the HBT radius parameters do not depend on the transverse momentum of the particle pair at all. To properly account for the observed m_T dependence of the radius parameters, one needs to invoke relativistic dynamics; for example, in the Buda-Lund parametrizations of Refs. [23,25] it turns out that the functional form of the dependence on particle mass m seen in Eqs. (38)–(43) is approximately conserved, just in the relativistic case, the dependence is on the transverse mass m_T of the particle pair. These parametrizations evolved to various hydrodynamical solutions; in particular the results in the present article can be considered as a nonrelativistic, rotating, and spheroidally symmetric Buda-Lund hydrodynamical solution. So, similarly to the remarks after Eq. (27), we conclude that as long as no relativistic description of the observables in a rotating system is available, our results give a hint at the proper dependence of the radius parameters on the kinematical variables by setting $m \rightarrow m_T$ in the formulas above.

As before, we illustrate the effects of rotation on the HBT radius parameters by taking a spherically symmetric initial

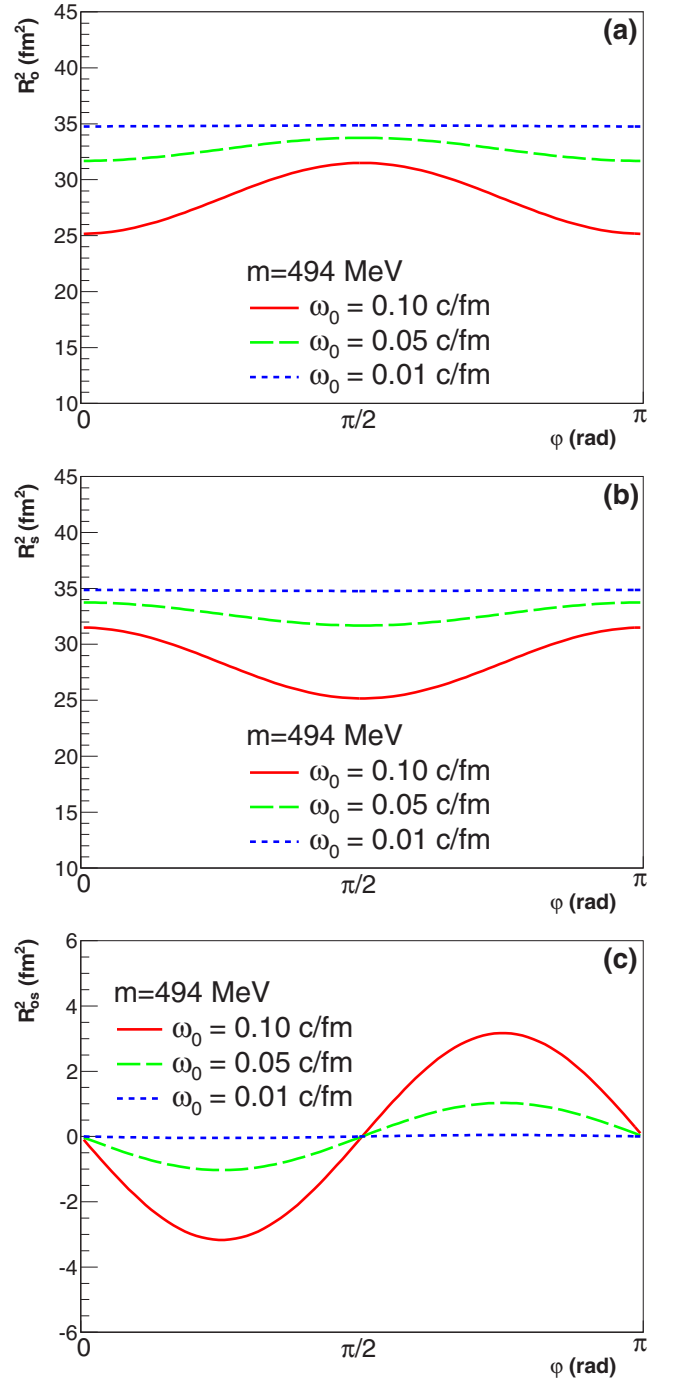


FIG. 7. HBT radius parameters R_o^2 (a), R_s^2 (b) and the cross-term R_{os}^2 (c) as a function of the azimuthal angle of the pair, at freeze-out. Initial conditions are the same as in Fig. 1, but this observable was calculated for charged kaons, with mass $m = 494$ MeV. The cases with three different ω_0 values illustrate the effect of rotation: it causes more anisotropy as well as an overall decrease of the magnitude of the azimuthally averaged radii.

condition with three different values of initial angular velocity. Fig. 7 shows the azimuthal angle dependence of R_o^2 , R_s^2 , and R_{os}^2 at the freeze-out time, while Fig. 8 shows the dependence of the azimuthal mean value of R_o^2 and R_l^2 on the freeze-out

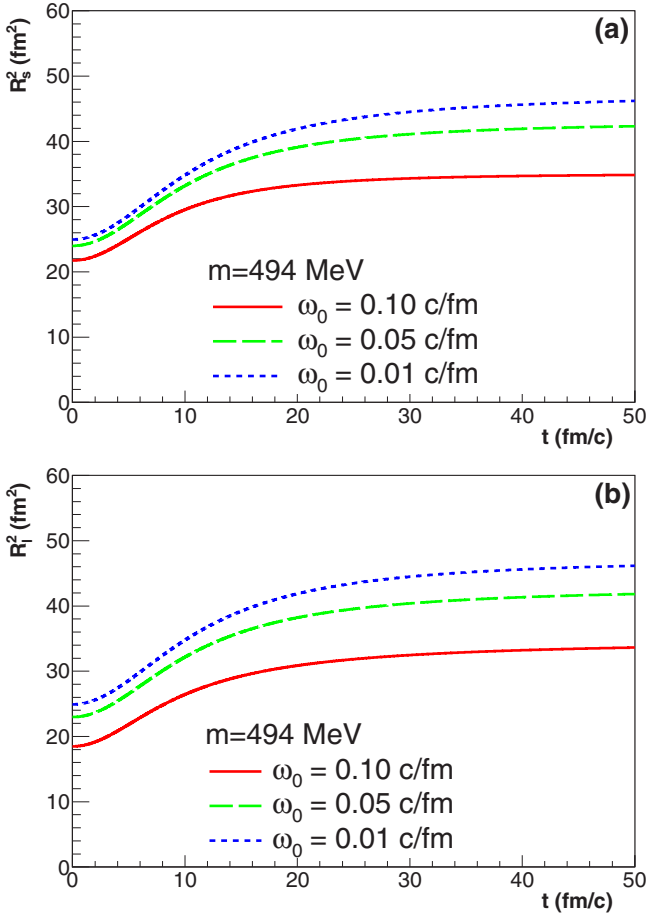


FIG. 8. Freeze-out time dependence of the azimuthal average of R_s^2 (a) and R_l^2 (c). Initial conditions are the same as in Fig. 1, and three different ω_0 values. This observable was calculated for charged kaons, with mass $m = 494$ MeV. Rotation decreases the magnitude of the radii.

time. (We plot only these ones, as the others are either not interesting or just very similar to these.) It is clearly seen that the overall magnitude of the azimuthal mean of the radius parameters decreases with rotation, as mentioned above. One also observes that all the oscillations become stronger with more rotation, a straightforward effect of anisotropic geometry stemming from the centrifugal force. This behavior is thus expected to be a general consequence of rotation.

IV. SUMMARY

We have evaluated the single-particle spectra, the elliptic and higher order flows, and the two-particle Bose-Einstein correlation functions for a rotating and expanding, spheroidally symmetric fireball; a non-relativistic Buda-Lund type hydrodynamical model. A nonvanishing value of the initial angular momentum—an important conserved quantity that is characteristic of noncentral heavy ion collisions—was taken into account, and its effects on the observables have been found using simple and straightforward analytic formulae. Although the hydrodynamical solution we used is nonrelativistic, the insight it gives into the observables

in rotating systems is valuable and relevant for analyzing experimental measurements of the treated observables.

We have proven that rotational terms appear in the observables in a way that is rather similar to radial flow effects and leads to the increased mass dependence of the effective temperatures or slope parameters of the single-particle spectra, an enhanced elliptic flow, and a stronger mass-dependence of the decrease of the Bose-Einstein correlation radii. We have illustrated these analytic results with several plots utilizing an academic but rather interesting spherical initial condition and initial angular velocities gradually increasing from a nearly vanishing value to a realistic value.

Using this special initial condition of a rotating and initially spherical fireball, we have demonstrated that initial angular momentum leads to a significant elliptic flow even for the case when there are no initial spatial asymmetries present. This implies that future experimental data analysis has to take possible rotational effects into account as they may mix in a subtle and difficult to identify manner with other, more generally considered radial flow effects.

We also emphasize that, to consider these important angular momentum and rotational effects, finite three-dimensional hydrodynamical solutions have to be utilized for the data analysis, as infinite systems have infinite moments of inertia so they cannot realistically model rotating hydrodynamical solutions.

ACKNOWLEDGMENTS

We gratefully acknowledge inspiring discussions with M. Csanád, L. Csernai, and Y. Hatta. The research of M.N. has been supported by the European Union and the State of Hungary, cofinanced by the European Social Fund in the framework of the TÁMOP 4.2.4 A/1-11-1-2012-0001 “National Excellence” Program. This work has been supported by the OTKA NK 101438 grant of the Hungarian National Science Fund.

APPENDIX A: EQUATIONS OF MOTION FOR $\kappa = 3/2$

For $\kappa = 3/2$, the solution of the equations of motion, Eq. (10), can be given using the Hamilton-Jacobi formalism, applied to the Hamiltonian (16). This formalism can be applied for a classical Hamiltonian $H(P_i, Q_i, t)$ as follows. (Here P_i and Q_i denote the N canonical momenta and coordinates.) One must find the classical Hamilton function, or action $S(Q_i, t)$, that is a solution of the Hamilton-Jacobi equation

$$\frac{\partial S}{\partial t} + H\left(\frac{\partial S}{\partial Q_i}, Q_i, t\right) = 0.$$

If a suitable solution $S(Q_i, t, K_i)$ is found, which has N different arbitrary parameters K_i , then the equations $\frac{\partial}{\partial K_i} S(Q_i, t, K_i) = L_i$, again with arbitrary constants L_i , give the solution of the equation of motion.

In cases where H is time dependent, the conserved energy E enters as a free parameter:

$$S(Q_i, t) = -Et + S(Q_i), \quad H\left(\frac{\partial S(Q_i)}{\partial Q_i}, Q_i\right) = E.$$

In our case, for $\kappa = 3/2$, we have

$$\frac{(\frac{\partial S}{\partial R})^2 + 2(\frac{\partial S}{\partial Y})^2}{4m} + \frac{m\omega_0^2 R_0^4}{R^2} + \frac{3T_0}{2} \left(\frac{R_0^2 Y_0}{R^2 Y} \right)^{\frac{2}{3}} = E.$$

This can be solved by introducing the ρ, χ variables (like planar cylindrical coordinates) as

$$R = \frac{\rho}{\sqrt{2}} \cos \chi, \quad Y = \rho \sin \chi$$

and rearranging the Hamilton-Jacobi equation to obtain

$$\left(\frac{\partial S}{\partial \rho} \right)^2 + \frac{1}{\rho^2} \left\{ \left(\frac{\partial S}{\partial \chi} \right)^2 + F(\chi) \right\} = 2mE,$$

with

$$F(\chi) = 2m^2 \omega_0^2 R_0^4 + 3mT_0 \left(\frac{2R_0^2 Y_0}{\cos^2 \chi \sin \chi} \right)^{2/3}.$$

The desired solution is now obtained straightforwardly, by introducing the constant K so that the equation becomes separable. We thus can assume that $S(\rho, \chi) = S_1(\rho) + S_2(\chi)$, and get the following solution:

$$\left(\frac{\partial S_1}{\partial \rho} \right)^2 + \frac{K}{\rho^2} = 2mE, \quad \left(\frac{\partial S_2}{\partial \chi} \right)^2 + F(\chi) = K \quad \Rightarrow$$

$$S = -Et + \int d\rho \sqrt{2mE - \frac{K}{\rho^2}} + \int d\chi \sqrt{K - F(\chi)}.$$

The equations of motion now can be considered solved. Taking the $\frac{\partial S}{\partial E} = B_1 = \text{const}$ condition, with elementary integration we get the following result:

$$\rho^2 = \frac{2E}{m} (t + B_1)^2 + \frac{K}{2mE}. \quad (\text{A1})$$

If one writes back R and Y in this result, and chooses the K and B_1 constants to match the initial conditions, one gets the following:

$$2R^2 + Y^2 = \frac{2E}{m} t^2 + (4\dot{R}_0 R_0 + 2\dot{Y}_0 Y_0) t + 2R_0^2 + Y_0^2, \quad (\text{A2})$$

where the E energy is in this case

$$\frac{E}{m} = \dot{R}_0^2 + \frac{\dot{Y}_0^2}{2} + \omega_0^2 R_0^2 + \frac{3T_0}{2m}.$$

Substituting E back in Eq. (A2), one readily arrives at Eq. (18). This gives the time dependence of $2R^2 + Y^2$. This result could have been inferred by simple inspection of the differential equations, and once this is known, a univariate differential equation also can be given (and numerically solved) for the remaining independent variables. This was known already in Refs. [19,24,30] (although not for a rotating system). Our method here gives the solution by quadratures; it is easy to see that the other condition coming from the Hamilton-Jacobi method, $\frac{\partial S}{\partial K} = B_2 = \text{const}$, does not contain the time variable t . So this condition fixes the shape of the trajectory in the R - Y "plane." However, in general it cannot be evaluated analytically.

APPENDIX B: A SURVEY OF ANALYTIC SOLUTIONS

In this Appendix we give a short list of some recent exact analytic solutions of the nonrelativistic hydrodynamical equations. We do this in the hope that, just as uniting efforts in heavy-ion physics and analytical hydrodynamics has been proven to be of great interest for both research directions, it can and will prove fruitful also in future applications (even though the heavy-ion physical applications of the mentioned solutions is not clear yet). In spite of the lack of basic mathematical theorems (such as existence and uniqueness) there are a fairly large number of analytic solutions available for various hydrodynamical equations, such as the Euler or the Navier-Stokes (NS) equations. As these are not well known in high-energy physics, we give a short overview about some of these recent developments in analytical hydrodynamics.

There are various examination techniques available, with numerous studies in the literature. Most of them are based on the application of the self-similar *Ansatz* or on Lie algebra methods.

Sedov in his classical work about self-similar solutions [31] presents one of the first analytic solutions for the three-dimensional spherical NS equation, where all three velocity components and the pressure have polar angle dependence (ϑ) only. Some similarity reduction solutions of the two-dimensional incompressible NS equation were presented by Xia-Yu [32]. Additional solutions are available for the (2+1)-dimensional NS equation also via symmetry reduction techniques in [33]. Manwai [34] studied the N -dimensional ($N \geq 1$) radial Navier-Stokes equation with different kinds of viscosity and pressure dependences, and presented analytical blow-up solutions. His works are still (1+1)-dimensional (one spatial and one time dimension) investigations.

In our former study we generalized the self-similar *Ansatz* of Sedov and presented analytic solutions for the most general three-dimensional Navier-Stokes equation in Cartesian coordinates [35]. The solutions are the Kummer functions with quadratic arguments. Later, we applied our method to the three-dimensional compressible NS equation where the politropic equation of state was used [36], resulting in the Whitakker functions.

Recently, Hu *et al.* [37] presented a study where symmetry reductions and exact solutions of the (2+1)-dimensional NS equation were presented. Aristov and Polyanin [38] use various methods, such as Crocco transformation, generalized separation of variables, or the method of functional separation of variables for the NS equation, and present large number of new classes of exact solutions.

A universal Lie algebra study is available for the most general three-dimensional NS equation [39]. Unfortunately, no explicit solutions are shown and analyzed there. Fushchich *et al.* [40] constructed a complete set of $\tilde{G}(1,3)$ -inequivalent *Ansätze* of codimension 1 for the NS system; they present 19 different analytical solutions for one or two space dimensions. Further, two- and three- dimensional studies based on the group theoretical method were presented by Grassi [41], getting Whitakker functions for solutions which are very similar to our results mentioned earlier [35].

- [1] L. P. Csernai, V. K. Magas, H. Stocker, and D. D. Strottman, *Phys. Rev. C* **84**, 024914 (2011).
- [2] L. Cifarelli, L. P. Csernai, and H. Stocker, *Europhys. News* **43**, 29 (2012).
- [3] L. P. Csernai, S. Velle, and D. J. Wang, *Phys. Rev. C* **89**, 034916 (2014).
- [4] L. P. Csernai and S. Velle, [arXiv:1305.0385](https://arxiv.org/abs/1305.0385).
- [5] S. Velle and L. P. Csernai, *Phys. Rev. C* **92**, 024905 (2015).
- [6] S. Velle, S. M. Pari, and L. P. Csernai, [arXiv:1508.04017](https://arxiv.org/abs/1508.04017).
- [7] T. Csörgő and M. I. Nagy, *Phys. Rev. C* **89**, 044901 (2014).
- [8] P. Csizmadia, T. Csörgő, and B. Lukács, *Phys. Lett. B* **443**, 21 (1998).
- [9] M. I. Nagy, *Phys. Rev. C* **83**, 054901 (2011).
- [10] Y. Hatta, J. Noronha, and B. W. Xiao, *Phys. Rev. D* **89**, 051702 (2014).
- [11] Y. Hatta, J. Noronha, and B. W. Xiao, *Phys. Rev. D* **89**, 114011 (2014).
- [12] B. McInnes, *Nucl. Phys. B* **887**, 246 (2014).
- [13] R. D. de Souza, T. Koide, and T. Kodama, *Prog. Part. Nucl. Phys.* **86**, 35 (2016).
- [14] F. Becattini, L. P. Csernai, and D. J. Wang, *Phys. Rev. C* **88**, 034905 (2013).
- [15] Y. Xie, R. C. Glastad, and L. P. Csernai, *Phys. Rev. C* **92**, 064901 (2015).
- [16] L. P. Csernai and J. H. Inderhaug, *Int. J. Mod. Phys. E* **24**, 1550013 (2015).
- [17] L. P. Csernai, D. J. Wang, and T. Csörgő, *Phys. Rev. C* **90**, 024901 (2014).
- [18] M. Baznat, K. Gudima, A. Sorin, and O. Teryaev, *Phys. Rev. C* **88**, 061901 (2013).
- [19] T. Csörgő, S. V. Akkelin, Y. Hama, B. Lukács, and Y. M. Sinyukov, *Phys. Rev. C* **67**, 034904 (2003).
- [20] K. Adcox *et al.* (PHENIX Collaboration), *Nucl. Phys. A* **757**, 184 (2005).
- [21] J. Adams *et al.* (STAR Collaboration), *Nucl. Phys. A* **757**, 102 (2005).
- [22] F. Becattini, M. Bleicher, T. Kollegger, T. Schuster, J. Steinheimer, and R. Stock, *Phys. Rev. Lett.* **111**, 082302 (2013).
- [23] M. Csanád, T. Csörgő, and B. Lörstad, *Nucl. Phys. A* **742**, 80 (2004).
- [24] T. Csörgő, *Acta Phys. Pol. B* **37**, 483 (2006).
- [25] T. Csörgő and B. Lörstad, *Phys. Rev. C* **54**, 1390 (1996).
- [26] T. Csörgő, *Heavy Ion Phys.* **15**, 1 (2002).
- [27] T. Csörgő, B. Lörstad, and J. Zimányi, *Phys. Lett. B* **338**, 134 (1994).
- [28] T. Csörgő, B. Lörstad, and J. Zimányi, *Z. Phys. C* **71**, 491 (1996).
- [29] Y. M. Sinyukov, *Nucl. Phys. A* **566**, 589C (1994).
- [30] S. V. Akkelin, T. Csörgő, B. Lukács, Y. M. Sinyukov, and M. Weiner, *Phys. Lett. B* **505**, 64 (2001).
- [31] L. Sedov, *Similarity and Dimensional Methods in Mechanics* (CRC Press, Boca Raton, 1993), p. 120.
- [32] J. Xia-Yu, *Commun. Theor. Phys.* **52**, 389 (2009).
- [33] K. Fakhar, T. Hayat, C. Yi, and N. Amin, *Commun. Theor. Phys.* **53**, 575 (2010).
- [34] Y. Manwai, *J. Math. Phys.* **49**, 113102 (2008).
- [35] I. F. Barna, *Commun. Theor. Phys.* **56**, 745 (2011).
- [36] I. F. Barna and L. Mátyás, *Fluid. Dyn. Res.* **46**, 055508 (2014).
- [37] X. R. Hu, Z. Z. Dong, F. Huang, and Y. Chen, *Z. Naturforsch. A* **65**, 504 (2010).
- [38] S. N. Aristov and A. D. Polyinin, *Russ. J. Math. Phys.* **17**, 1 (2010).
- [39] V. N. Grebenev, M. Oberlack, and A. N. Grishkov, *J. Nonlin. Math. Phys.* **15**, 227 (2008).
- [40] W. I. Fushchich, W. M. Shtelen, and S. L. Slavutsky, *J. Phys. A: Math. Gen.* **24**, 971 (1990).
- [41] V. Grassi, R. A. Leo, G. Soliani, and P. Tempesta, *Physica* **286**, 79 (2000); **293**, 421 (2000).